Structure and Transport Properties of the $LiPF_6$ Doped 1-Ethyl-2,3-dimethyl-imidazolium Hexafluorophosphate Ionic Liquids: A Molecular Dynamics Study

Shuai Niu, Zhen Cao, Shu Li, and Tianying Yan*

Institute of New Material Chemistry, Department of Material Chemistry, and Institute of Scientific Computing, Nankai University, Tianjin 300071, China

Received: October 2, 2009; Revised Manuscript Received: November 7, 2009

Molecular dynamics simulations have been performed on 1-ethyl-2,3-dimethyl-imidazolium hexafluorophosphate ($EMMIPF_6$) ionic liquids (ILs) doped with different molar ratios of $LiPF_6$ at 523.15 K and 1 bar. Ionic conductivity, self-diffusion coefficients, density, and viscosity predicted by MD simulations were found to be in good agreement with previous studies. Structural analysis shows that the Li^+ cation is strongly coordinated by the F atom of the PF_6^- anion, and the number of F atoms coordinated with a Li^+ cation in the first solvation shell is about six for all molar ratios of $LiPF_6/EMMIPF_6$ 0.05, 0.15, 0.30, and 0.50. The coordination number of the PF_6^- anion within the first solvation shell of Li^+ cation is about four, which tends to increase slightly when the salt concentration is increased. The two-dimensional radial-angular distribution study shows that the $Li^+-PF_6^-$ complex tends to form the C_{2v} conformation at low salt concentration, whereas C_{4v} conformation becomes important at higher salt concentration. It is found that the aggregation of $Li^+-PF_6^-$ complexes occurs in all four molar ratios, whereas ionic conductivity decreases and viscosity increases at higher salt concentration. The residence time correlation of PF_6^- within the first solvation shell of Li^+ shows a strong memory effect. The Li^+-hopping function further shows that the hopping of Li^+ is strongly affected by its environment with different exchange rates of the PF_6^- anions for the structure diffusion, and the system of 0.5 $LiPF_6/EMMIPF_6$ molar ratio has the slowest hopping rate.

I. Introduction

Rechargeable lithium batteries, with liquid electrolytes, are extensively used in portable electronic devices, such as cell phones and laptop computers.[1−3] Ionic liquids (ILs), composed of imidazolium or pyrrolidinium cations and hexafluorophosphate (PF_6^-) or trifluoromethanesulfonylimide ($TFSI^-$) anions, doped by the lithium salt $LiPF_6$ or LiTFSI, are widely studied[4−8] because of the excellent capabilities of these ILs in dissolving lithium salts and transporting Li^+ cations as well as the negligible vapor pressure with wide liquid-phase ranges.[9−11] To design better lithium batteries for practical use, certain compromise has to be made between the increase in the lithium charge carrier concentration and the concomitant increase in the viscosity and resistivity.[4,12] Moreover, a variety of properties such as electrochemical and thermal stabilities, safety, and environmental compatibility as well as some well-entrenched requirements such as high conductivity and transference number, low flammability, volatility, and toxicity must be carefully and comprehensively investigated and optimized.[13−16]

The detailed structural and ion transport properties of imidazolium-based ILs play a pivotal role in recent studies.[12,17−19] ILs containing 1,3-dialkylimidazolium cation and PF_6^- anion have been studied as solvents in lithium batteries.[17,18] However, the presence of an acidic proton on the carbon atom C2 of the imidazolium ring (cf. Figure 1, in which an H atom instead of a methyl group is bonded to the C2 atom) precludes the good performance of the batteries because of its instability of Li.[20−22] Therefore, introducing an alkyl group at the C2 position enhances the electrochemical stability and yields attractive electrolytes for lithium batteries. Given these scenarios, 1-ethyl-2,3-dimethyl-imidazolium cation (cf. Figure 1) is a good choice in bringing satisfying performance in lithium batteries.[12,23] Likewise, the PF_6^- anion is employed because it would result in the solvents with high ion dissociation and conductivity.[4,24] To determine the Li^+ cation environment and its transport mechanism in lithium batteries, molecular dynamics (MD) simulation is essential in exploring structure and transport properties in lithium salt-doped ILs.[25]

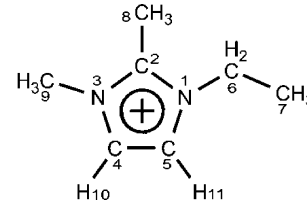

Figure 1. Schematic structure of the 1-ethyl-2,3-dimethyl-imidazolium ($EMMI^+$) cation.

In this study, we performed MD simulation on IL 1-ethyl-2,3-dimethyl-imidazolium hexafluorophosphate ($EMMIPF_6$) doped by $LiPF_6$ as nonaqueous electrolyte system at four different $LiPF_6/EMMIPF_6$ molar ratios, namely, 0.05, 0.15, 0.30, and 0.50. $EMMI^+$ was introduced here as solvent ion because of its high dissociation constants.[26] Considering the melting temperature of $EMMIPF_6$ at 469.15 K,[27] the simulations were performed at 523.15 K, and it may serve as electrolyte working at intermediate high temperature. The structural and Li^+ transportation properties are studied by MD simulation on a nanosecond time scale.

II. Molecular Dynamics Simulation Methodology

We used an all-atom, all-flexible model in this study with a classical force field that takes the standard form

* To whom correspondence should be addressed: E-mail: tyan@nankai.edu.cn.

10.1021/jp909486z
Published on Web 11/23/2009

$$V = \sum_{\text{bonds}} k_b(r - r_0)^2 + \sum_{\text{angles}} k_\theta(\theta - \theta_0)^2 + \sum_{\text{dihedrals}} V_n[1 + \cos(n\varphi - \delta)] + \sum_i \sum_{j>i} \left\{ 4\varepsilon \left[\left(\frac{\sigma}{r_{ij}}\right)^{12} - \left(\frac{\sigma}{r_{ij}}\right)^{6} \right] + \frac{1}{4\pi\varepsilon_0} \frac{q_i q_j}{r_{ij}} \right\} \quad (1)$$

In brief, the above potential energy function includes intramolecular bond stretching, angle bending, and dihedral angle torsional motion as well as long-range Lennard-Jones and Coulombic interactions. Because of the relatively long simulation time (50 ns for the production run), a pairwise-based Fennell and Gezelter shifted force (FGSF) method[28,29] is employed to handle the Coulombic interactions. In the previous study of an imidazolium-based IL system, it was demonstrated that the FGSF method is roughly eight times faster than the standard Ewald sum method,[30] with no loss of accuracy.[31] The radial cutoff distance for the van der Waals and Coulombic interaction was 12 Å. The force-field parameters for lithium were taken from the AMBER force field,[32] and those for $EMMI^+$ and PF_6^- were taken from Pádua et al.[19,23,33] The simulation was performed with an "in-house" MD code.

Four $LiPF_6$/$EMMIPF_6$ nonaqueous electrolyte models, with different $LiPF_6$/$EMMIPF_6$ molar ratios, namely, 0.05, 0.15, 0.30, 0.50, were simulated in this study. The number of ions of each model, altogether with the PBC cell lengths, are listed in Table 1. These systems were initially created in a sufficiently large cubic cell with periodic boundary conditions. The systems were equilibrated with isobaric−isothermal (NPT) simulation,[34,35] coupled to a barostat of 1 bar pressure and a thermostat of 523.15 K[36] by annealing the systems gradually from 1000 to 523.15 K in 10 ns, with an integration time step 1 fs. Subsequently, 50 ns NPT production runs were performed for each system, and phase space data were recorded every 1 ps. The average densities were 1.21, 1.24, 1.31, and 1.44 g/cm^3, respectively, for the $LiPF_6$/$EMMIPF_6$ molar ratios 0.05, 0.15, 0.30, and 0.50, as listed in Table 1. Therefore, density increases as the salt concentration increases.

III. Results and Discussion

Figure 2 shows the atomic site−site partial radial distribution functions (RDFs), $g_{ij}^{ss}(r)$, and the corresponding cumulative distribution functions (CDFs), $n_{ij}^{ss}(r)$, where

$$g_{ij}^{ss}(r) = \frac{<\sum_{ij} \delta(r - r_{ij})>}{4\pi r^2 \rho_j \, dr} \quad (2)$$

and

$$n_{ij}^{ss}(r) = \rho_j \int_0^r 4\pi r'^2 g_{ij}^{ss}(r') \, dr' \quad (3)$$

For the atomic site−site RDFs, g_{ij}^{ss}, r_{ij} in eq 2 denotes the distance between the Li^+ cation and other atoms, and ρ_j is the number density of the jth atom in the system. The g_{ij}^{ss} and n_{ij}^{ss} are denoted by solid and dashed-dotted lines, respectively, in Figure 2. It can be seen from g_{ij}^{ss} that the Li^+ cation is strongly coordinated by the F atoms of the PF_6^- anion in all four systems. The peaks in Figure 2a,b appear at the same position, respectively, which is marginally affected by the $LiPF_6$ salt concentration. Bimodal peak is found in Li−P and Li−F g_{ij}^{ss} within the first solvation shell (5.0 Å of the first minimum of Li−P RDF for all four systems), indicating that multiple PF_6^- anions coordinate to the Li^+ cation. The corresponding n_{ij}^{ss} of Li−P and Li−F in Figure 2a,b shows that the coordination number of the F atoms within the first solvation shell of Li^+ cation (2.8 Å) is about 6 for the 0.05, 0.15, 0.30, and 0.50 $LiPF_6$ molar ratio systems. From Figure 2a, it can be seen that the coordination number of PF_6^- anion around one Li^+ cation is about four, which increases slightly as the lithium salt concentration is enhanced. The combination of the deep minimum of g^{ss}_{Li-P} and the shallow minimum of g^{ss}_{Li-F} suggests the rotation of the spherical PF_6^- around Li^+, which changes the Li^+−F coordinations.

TABLE 1: Numbers of Li^+, $EMMI^+$, and PF_6^- for Each Simulation of Different $LiPF_6$ Molar Ratios As Well As the Corresponding Density and the PBC Cell Length

$LiPF_6$ molar ratio	Li^+	$EMMI^+$	PF_6^-	PBC cell length (Å)	ρ(g/cm^3)
0.05	9	169	178	40.11	1.21
0.15	29	164	193	40.18	1.24
0.30	66	154	220	40.27	1.31
0.50	135	135	270	40.38	1.44

When a Li^+ cation is coordinated with a PF_6^- anion, the angle ∠Li−P−F′, where F′ is the nearest F atom to the Li^+ cation, is 45, 54.7, and 0°, respectively, for C_{2v}, C_{3v}, C_{4v} symmetry. Figure 3 shows the 2D distribution of Li−P radial and ∠Li−P−F′ angular distributions of the four different salt concentrations. It can be seen that Li−PF_6 complexes are most likely to form C_{2v} conformation with ∠Li−P−F′ around 41° to 42° and Li−P distance 2.86 to 2.90 Å in all $LiPF_6$ concentrations studied here. As $LiPF_6$/$EMMIPF_6$ molar ratio reaches 0.5, a C_{4v} peak appears at (14.2°, 3.47 Å). It is notable that no obvious gas-phase minimum C_{3v} conformation is observed, which is in agreement with previous studies.[4,24] A PF_6^- anion donates three, two, or one F atom to coordinate with Li when it behaves as the C_{3v}, C_{2v}, or C_{4v} symmetry, respectively. To coordinate with multiple PF_6^- anions in the condensed phase, the Li−PF_6 complex is more likely to form the C_{2v} or C_{4v} symmetry for the coordination number of P atom of about four. Given the scenario that the coordination number of the P atoms around a Li^+ cation slightly increases as the Li^+ concentration is enhanced, it is reasonable that to keep a coordination number of six, each PF_6^- anion tends to donate fewer F atoms to participate the coordination when the total number of PF_6^- around one Li^+ cation is accumulating.

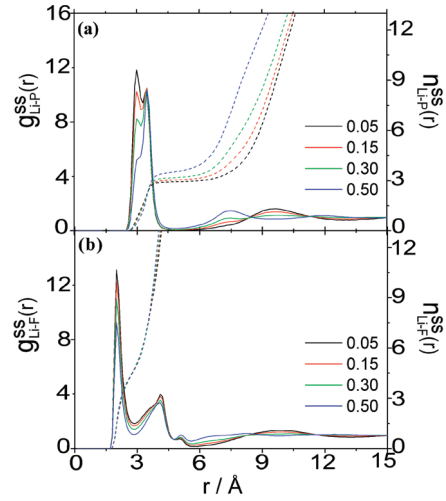

Figure 2. Atomic site−site partial radial distribution functions (RDFs), g_{ij}^{ss}, and the corresponding cumulative distribution functions (CDFs), n_{ij}^{ss}, of (a) Li^+−P(PF_6^-) and (b) Li^+−F(PF_6^-). Black, red, green, and blue lines denote the 0.05, 0.15, 0.30, and 0.50 $LiPF_6$ molar ratio systems, respectively. The solid lines represent g_{ij}^{ss}, and the dashed-dotted lines represent n_{ij}^{ss}.

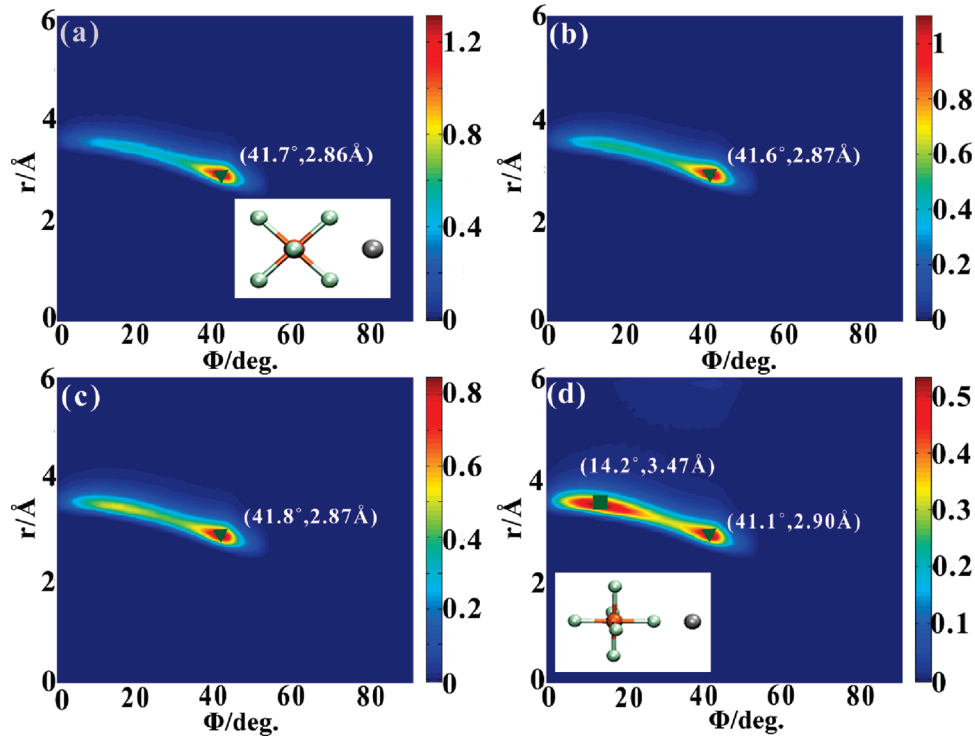

Figure 3. Two-dimensional radial-angular distribution of $Li^+-P(PF_6^-)$ distance and ∠Li−P−F′, in which F′ is the nearest F atom to the Li^+ cation, of different $LiPF_6$ molar ratios: (a) 0.05, (b) 0.15, (c) 0.30, and (d) 0.50. The insets in parts a and d demonstrate the C_{2v} and C_{4v} conformation of the $Li^+-PF_6^-$ complex, respectively.

TABLE 2: Viscosity (η), Self-Diffusion Coefficient (D), Uncorrelated Conductivity (λ_{uncorr}), Ionic Conductivity (λ), and the Degree of Uncorrelated Ion Motion (α) of Different $LiPF_6$ Molar Ratios

system ($LiPF_6$ molar ratio)	η (c.p)[a]	D (10^{-5} cm^2/s)[b]	λ(S/cm)[c]	λ_{uncorr} (S/cm)[d]	α[e]
0.05	3.22 ± 0.14	0.20, 0.43, 0.31	0.067	0.072	0.93
0.15	5.34 ± 0.16	0.16, 0.39,0.25	0.051	0.064	0.80
0.30	10.73 ± 0.58	0.10, 0.28, 0.15	0.040	0.045	0.90
0.50	20.07 ± 0.80	0.042, 0.15, 0.060	0.019	0.023	0.81

[a] $\eta = \lim_{t\to\infty} ((V)/(20k_BTt))\langle\sum_{\alpha,\beta}(L_{\alpha\beta}(t) - L_{\alpha\beta}(0))^2\rangle$,[4] in which $L_{\alpha\beta}(t) = \int_0^t P_{\alpha\beta}(t')\,dt'$, k_B is the Boltzmann constant, T is temperature, t is time, V is the volume of the simulation box, and $P_{\alpha\beta}$ is the symmetrized and traceless stress tensor given by $P_{\alpha\beta} = \omega_{\alpha\beta}(((\sigma_{\alpha\beta} + \sigma_{\beta\alpha})/2) - (\delta_{\alpha\beta}/3)tr(\sigma))$, in which $\sigma_{\alpha\beta}$ is the stress tensor and $\omega_{\alpha\beta} = 1$ for $\alpha \neq \beta$, and $\omega_{\alpha\beta} = 4/3$ for $\alpha = \beta$, whereas $\delta_{\alpha\beta} = 1$ for $\alpha = \beta$ and $\delta_{\alpha\beta} = 0$ for $\alpha \neq \beta$. Error bars are estimated at 95% confidence interval, with standard deviation calculated by the slopes at 200 to 250 ps from MSDs of the time integration of the symmeterized and traceless stress tensor, $L_{\alpha\beta}(t)$. (See Figure S1 of the Supporting Information.) [b] $D_i = \lim_{t\to\infty} (1/6t)\langle|R_i(t) - R_i(0)|^2\rangle$, in which $|R_i(t) - R_i(0)|^2$ is the mean-square displacement of the center of mass of a molecule of species i during time t and $\langle\rangle$denotes the ensemble average. The diffusion coefficients listed are D_{Li^+}, D_{EMMI^+}, and $D_{PF_6^-}$, respectively. The MSDs are presented in Figure S2 of the Supporting Information. [c] $\lambda = \lim_{t\to\infty} (e^2/(6tVk_BT))\sum_{ij}^N z_i z_j\langle[R_i(t) - R_i(0)][R_j(t) - R_j(0)]\rangle$,[4,40] where e is the electron unit charge, V is the volume of the simulation box, k_B is the Boltzmann constant, T is the temperature, t is time, z_i and z_j are the partial charges carried by ions i and j, $R_i(t)$ is the displacement of the ion i during time t, N is the total number of ions in the simulation box, and $\langle\rangle$denotes the ensemble average. Total charge MSDs are presented in Figure S3 of the Supporting Information. [d] $\lambda_{uncorr}(t) = (e^2/(Vk_BT))(n_{Li^+}D_{Li^+} + n_{EMMI^+}D_{EMMI^+} + n_{PF_6^-}D_{PF_6^-}) = \lim_{t\to\infty} (e^2/(6tVk_BT))\sum_i^N z_i^2\langle[R_i(t) - R_i(0)]^2\rangle$. [e] $\alpha = \lambda/\lambda_{uncorr}$.

Therefore, the preference of C_{2v} and C_{4v} symmetry with different Li^+ concentration is dominant in liquid electrolyte system.

Viscosity (η), self-diffusion coefficient (D), uncorrelated conductivity (λ_{uncorr}), ionic conductivity (λ), and the degree of uncorrelated ion motion (α) of different species of all four systems are listed in Table 2. Increasing the lithium salt content results in a diminution of D for all species, and this is consistent with the fact that the viscosity increases and conductivity decreases with higher lithium salt concentration. The order of the diffusion coefficient is $EMMI^+ > PF_6^- > Li^+$. The $EMMI^+$ cation, despite being relatively bulky and asymmetric, diffuses faster than the spherical PF_6^- anion and small Li^+ cation. The fastest diffusion coefficient of the $EMMI^+$ suggests that neither the Li^+ cation nor the PF_6^- anion is likely to diffuse as a single ion but diffuse together as aggregate to a certain extent as a result of the strong interactions between these two species, as suggested by the previous studies.[4,12,24] The degree of uncorrelated ion motion (α) is typically measured as the ratio of the collective (total) charge transport (given by λ) to the charge transport due to self-diffusion only (a limit of uncorrelated motion) λ_{uncorr}. It can been seen in Table 2 that α is smaller than 1 for all salt concentrations, indicating the correlated motions of the $Li^+-PF_6^-$ aggregates and thus do not contribute to the conductivity. It is also notable that under the simulation temperature in this study, namely, 523.15 K, the conductivities of all four systems reach a magnitude of 10^{-2} S/cm order, which agree with other studies with similar electrolyte systems,[12] highlighting their potential applications in lithium batteries.

To investigate the Li^+ transport properties, the PF_6^- anion residence time in the first solvation shell of Li^+ is investigated. The residence time autocorrelation function $C(t)$ of the PF_6^- anion was calculated with the following expression[37]

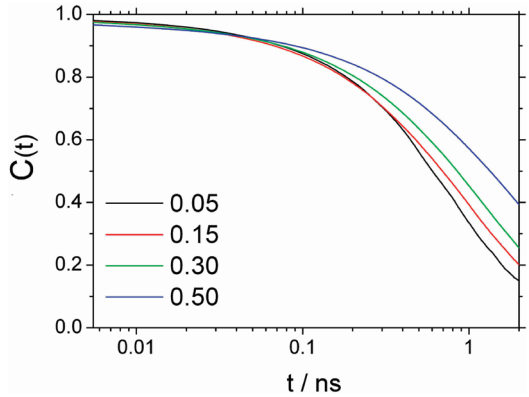

Figure 4. Residence time correlation function of the PF_6^- anion within the first solvation shell of the Li^+ cation of different $LiPF_6$ molar ratios.

$$C(t) = \frac{\langle H_{ij}(t)H_{ij}(0)\rangle}{\langle H_{ij}(0)H_{ij}(0)\rangle} \tag{5}$$

in which $H_{ij}(t)$ is 1 if the distance between Li^+ cation, i, and P of the PF_6^- anion, j, is within 5.0 Å, that is, the first minimum in Figure 2a and zero otherwise, and $\langle\rangle$ denotes average over all the time origins. $C(t)$ values of four different salt concentrations are shown in Figure 4. It can be seen that the system of higher $LiPF_6$ concentration decays slower than the lower salt concentrations, which is consistent with the higher viscosity and lower conductivity of higher salt concentration in Table 2. Although a relatively high temperature, 523.15 K, was employed in this simulation, $C(t)$ values of the whole system still retain strong memory effect, and all of them do not decay to zero at 2 ns. Therefore, the first solvation shell around a Li^+ cation is very stable, and the center Li^+ cation is likely to diffuse altogether with its surrounding PF_6^- anions.

To study the Li^+-hopping rate further, we described the trajectory of Li^+ cation by a hopping function $h(t)$, that is[38]

$$h(t) = h(t - \Delta t) + \Delta h(t) \tag{6}$$

where Δt is taken to be 5 ps, and

$$\Delta h(t) = \begin{cases} 0, \text{ if a taged } Li^+\text{cation maintains its coordinated } PF_6^- \text{at time } t \\ 1, \text{ if a taged } Li^+\text{cation changes its coordinated } PF_6^- \text{at time } t \\ -1, \text{ if a taged } Li^+\text{cation recoordinated with prior } PF_6^- \text{at time } t \end{cases} \tag{7}$$

It should be mentioned that the addition of a new PF_6^- anion to the first solvation shell of Li^+ does not break the original coordinated PF_6^- anions, and $\Delta h(t) = 0$ in that case. The $h(t)$ values for a randomly selected Li^+ of all four systems are shown in Figure 5, which demonstrates how the first solvation shell of the Li^+ cation is dynamically broken and formed. It is clear that the oscillatory Li^+ shuttling occurs quite infrequently, especially during the "long-resting" periods, as denoted by the pink ellipse, when little or no forward Li^+-hopping takes place. During "fast-jumping" periods, as denoted by the green ellipse, a substantial number of hops were observed but with little oscillatory shuttling. Such phenomenon highlights the fact that the hopping of Li^+ is strongly affected by its environment with different exchange rates of the PF_6^- anions for the structure diffusion[9] and the dynamical heterogeneity[39] in the Li^+ transportation because the Li^+ cations may be trapped in its solvation shell for very long time. The hopping rate of the Li^+ cation is found to be significantly slower in the IL with higher concentration of the $LiPF_6$/$EMMIPF_6$ molar ratio 0.5, indicating a strong

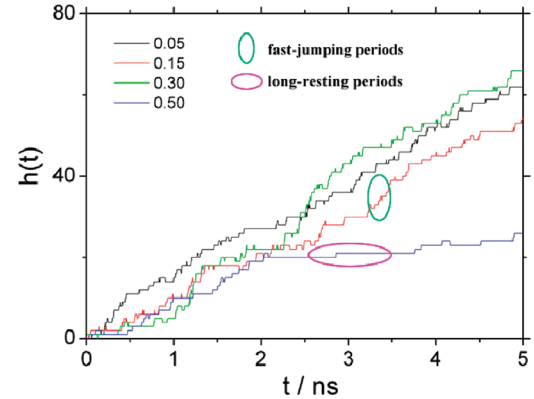

Figure 5. Hopping function of a randomly selected Li^+ for all four systems with different $LiPF_6$ molar ratios. The green ellipse denotes the fast-jumping periods, and the pink one denotes the long-resting periods.

aggregation of $Li^+-PF_6^-$ at such high salt concentration, and the Li^+ cations involved in the $Li^+-(PF_6^-)_n$ clusters tend to diffuse together with the clusters at a significantly slower rate than the Li^+ cations that are not in the aggregates.

IV. Summary

In this study, MD simulations were performed on IL electrolyte $LiPF_6$/$EMMIPF_6$ systems with different $LiPF_6$ molar ratios of 0.05, 0.15, 0.30, and 0.50. Structural analysis shows that the Li^+ cation is strongly coordinated by the F atom from the PF_6^- anion, and the coordination number of the F atoms around a Li^+ cation is about six for all four different molar ratios employed in this study. In the mean time, the most possible coordination number of the PF_6^- anion around one Li^+ cation is four, which tends to increase slightly when the $LiPF_6$ concentration increases. The 2D radial-angular distribution study shows that the $Li^+-PF_6^-$ complex tends to form C_{2v} or C_{4v} conformation but not the gas-phase most stable C_{3v} conformation. Such observation is in good agreement with the previous studies on the similar electrolytes.[4,24] The probability of forming the C_{4v} conformation is enhanced at higher $LiPF_6$ concentration. Study on the transport properties shows the formation of $Li^+-PF_6^-$ aggregates in the systems because of the fact that the degree of uncorrelated ion motion is smaller than 1 and that $EMMI^+$ has the highest diffusion coefficient. It is found that the viscosity increases and conductivity decreases at higher salt concentration, and the Li^+ cation retains the long time memory of its coordination PF_6^- anions. Further analysis on the hopping of Li^+ indicates that the transportation of Li^+ cations is decreased with the increment of the concentration of the $LiPF_6$. In addition, the Li^+ cation has a similar hopping rate for the $LiPF_6$/$EMMIPF_6$ molar ratio up to 0.3, whereas the 0.5 molar ratio significantly retards the Li^+ hopping rate.

Acknowledgment. This work is supported by NSFC (20503013, 20873068), the 973 Program (2009CB220100), and the 863 Program (2007AA03Z225) of China. We are grateful to Professor Agílio A. H. Pádua for the force field parameters of $EMMI^+$.

Supporting Information Available: Mean square displacement (MSD) of the time integration of the symmetrized and traceless stress tensor, MSD of the individual ions, and total charge MSD. This material is available free of charge via the Internet at http://pubs.acs.org.

References and Notes

(1) Xu, K. *Chem. Rev.* **2004**, *104*, 4303.
(2) Guidotti, R. A.; Masset, P. *J. Power Sources* **2006**, *161*, 1443.
(3) Armand, M.; Tarascon, J. M. *Nature* **2008**, *451*, 652.
(4) Borodin, O.; Smith, G. D. *J. Phys. Chem. B* **2009**, *113*, 1763.
(5) Roux, C.; Sanchez, J.-Y. *Electrochim. Acta* **1995**, *40*, 953.
(6) Kaur, D. P.; Yamada, K.; Park, J. S.; Sekhon, S. S. *J. Phys. Chem. B* **2009**, *113*, 5381.
(7) Borodin, O.; Smith, G. D. *J. Phys. Chem. B* **2006**, *110*, 6293.
(8) Borodin, O.; Smith, G. D. *J. Phys. Chem. B* **2006**, *110*, 6279.
(9) Borodin, O.; Smith, G. D. *J. Phys. Chem. B* **2006**, *110*, 4971.
(10) MacFarlane, D. R.; Meakin, P.; Sun, J.; Amini, N.; Forsyth, M. *J. Phys. Chem. B* **1999**, *103*, 4164.
(11) Henderson, W. A.; Herstedt, M.; Young, V. G.; Passerini, S.; De Long, H. C.; Trulove, P. C. *Inorg. Chem.* **2006**, *45*, 1412.
(12) Monteiro, M. J.; Bazito, F. F. C.; Siqueira, L. J. A.; Ribeiro, M. C. C.; Torresi, R. M. *J. Phys. Chem. B* **2008**, *112*, 2102.
(13) Borodin, O.; Smith, G. D. *J. Solution Chem.* **2007**, *36*, 803.
(14) Sakaebe, H.; Matsumoto, H. *Electrochem. Commun.* **2003**, *5*, 594.
(15) Lassègues, J. C.; Grondin, J.; Aupetit, C.; Johansson, P. *J. Phys. Chem. A* **2009**, *113*, 305.
(16) Borodin, O.; Smith, G. D. *Macromolecules* **2006**, *39*, 1620.
(17) Li, S.; Cao, Z.; Peng, Y. X.; Liu, L.; Wang, Y. L.; Wang, S.; Wang, J. Q.; Yan, T. Y.; Gao, X. P.; Song, D. Y.; Shen, P. W. *J. Phys. Chem. B* **2008**, *112*, 6398.
(18) Valoen, L. O.; Reimers, J. N. *J. Electrochem. Soc.* **2005**, *152*, A882.
(19) Bhargava, B. L.; Balasubramanian, S. *J. Chem. Phys.* **2007**, *127*, 114510.
(20) Bazito, F. F. C.; Kawano, Y.; Torresi, R. M. *Electrochim. Acta* **2007**, *52*, 6427.
(21) Koch, V. R.; Nanjundiah, C.; Battista Appetecchi, G.; Scrosati, B. *J. Electrochem. Soc.* **1995**, *142*, L116.
(22) J. Fuller, R. T. C.; Osteryoung, R. A. *J. Electrochem. Soc.* **1997**, *144*, 3881.
(23) Lopes, J. N. C.; Pádua, A. A. H.; Shimizu, K. *J. Phys. Chem. B* **2008**, *112*, 5039.
(24) Borodin, O.; Smith, G. D.; Jaffe, R. L. *J. Comput. Chem.* **2001**, *22*, 641.
(25) Borodin, O.; Smith, G. D. *J. Phys. Chem. B* **2006**, *110*, 16879.
(26) Ye, C.; Shreeve, J. M. *J. Phys. Chem. A* **2007**, *111*, 1456.
(27) Galiński, M.; Lewandowski, A.; Stepniak, I. *Electrochim. Acta* **2006**, *51*, 5576.
(28) Wolf, D.; Keblinski, P.; Phillpot, S. R.; Eggebrecht, J. *J. Chem. Phys.* **1999**, *110*, 8254.
(29) Fennell, C. J.; Gezelter, J. D. *J. Chem. Phys.* **2006**, *124*, 234104.
(30) Allen, M. P.; Tildesley, D. J. *Computer Simulation of Liquids*; Oxford: New York, 1987.
(31) Shi, W.; Maginn, E. J. *J. Phys. Chem. B* **2008**, *112*, 2045.
(32) Cornell, W. D.; Cieplak, P.; Bayly, C. I.; Gould, I. R.; Merz, K. M.; Ferguson, D. M.; Spellmeyer, D. C.; Fox, T.; Caldwell, J. W.; Kollman, P. A. *J. Am. Chem. Soc.* **1995**, *117*, 5179.
(33) Lopes, J. N. C.; Deschamps, J.; Pádua, A. A. H. *J. Phys. Chem. B* **2004**, *108*, 11250.
(34) Martyna, G. J.; Tobias, D. J.; Klein, M. L. *J. Chem. Phys.* **1994**, *101*, 4177.
(35) Martyna, G. J.; Tuckerman, M. E.; Tobias, D. J.; Klein, M. L. *Mol. Phys.* **1996**, *87*, 1117.
(36) Hoover, W. G. *Phys. Rev. A* **1985**, *31*, 1695.
(37) Borodin, O.; Smith, G. D.; Fan, P. *J. Phys. Chem. B* **2006**, *110*, 22773.
(38) Chen, H.; Yan, T.; Voth, G. A. *J. Phys. Chem. A* **2009**, *113*, 4507.
(39) Del Pópolo, M. G.; Voth, G. A. *J. Phys. Chem. B* **2004**, *108*, 1744.
(40) Borodin, O.; Smith, G. D. *J. Phys. Chem. B* **2006**, *110*, 11481.

JP909486Z